Clearance Kinetics and Clearance Routes of Molecules From the Suprachoroidal Space After Microneedle Injection

Bryce Chiang,[1] Ke Wang,[1] C. Ross Ethier,[1] and Mark R. Prausnitz[1,2]

[1]Wallace H. Coulter Department of Biomedical Engineering at Georgia Tech and Emory University, Georgia Institute of Technology, Atlanta, Georgia, United States
[2]School of Chemical and Biomolecular Engineering, Georgia Institute of Technology, Atlanta, Georgia, United States

Correspondence: Mark R. Prausnitz, School of Chemical and Biomolecular Engineering, Georgia Institute of Technology, 311 Ferst Drive, Atlanta, GA 30332, USA; prausnitz@gatech.edu.

Submitted: September 3, 2016
Accepted: November 22, 2016

Citation: Chiang B, Wang K, Ethier CR, Prausnitz MR. Clearance kinetics and clearance routes of molecules from the suprachoroidal space after microneedle injection. *Invest Ophthalmol Vis Sci*. 2017;58:545–554. DOI: 10.1167/iovs.16-20679

Purpose. To determine clearance kinetics and routes of clearance of molecules from the suprachoroidal space (SCS) of live New Zealand White rabbits.

Methods. Suprachoroidal space collapse rate and pressure changes after microneedle injection into SCS were determined. Fluorescent fundus images were acquired to determine clearance rates of molecules ranging in size from 332 Da to 2 MDa. Microneedle injections of fluorescein were performed, and samples were taken from various sites over time to determine amount of fluorescein exiting the eye. Clearance transport was modeled theoretically and compared with experimental data.

Results. After injection, pressures in SCS and vitreous humor spiked and returned to baseline within 20 minutes; there was no difference between these two pressures. Suprachoroidal space collapse occurred within 40 minutes. One hour after fluorescein injection, 46% of fluorescein was still present in the eye, 15% had transported across sclera, 6% had been cleared by choroidal vasculature, and 4% had exited via leakage pathways. Characteristic clearance time increased in proportion with molecular radius, but total clearance of 2 MDa FITC-dextran was significantly slower (21 days) than smaller molecules. These data generally agreed with predictions from a theoretical model of molecular transport.

Conclusions. Guided by experimental data in the context of model predictions, molecular clearance from SCS occurred in three regimes: (1) on a time scale of approximately 10 minutes, fluid and molecules exited SCS by diffusion into sclera and choroid, and by pressure-driven reflux via transscleral leakage sites; (2) in approximately 1 hour, molecules cleared from choroid by blood flow; and (3) in 1 to 10 hours, molecules cleared from sclera by diffusion and convection.

Keywords: ophthalmic drug delivery kinetics, suprachoroidal space of eye, microneedle injection, transscleral clearance, perivascular drainage, injection site reflux, random walk model

Suprachoroidal drug delivery is an emerging route of administration that targets diseased tissues in posterior segment diseases, such as AMD and uveitis.[1–4] Because the suprachoroidal space (SCS) is bounded by the ciliary body, choroid, and sclera, significantly higher bioavailability at these tissues can be achieved with SCS delivery compared with eye drops or intravitreal (IVT) injections,[5–9] leading to significant dose sparing for drugs with a site of action at these tissues.[10–12] Fewer ocular side effects are expected due to dose sparing and also because drugs are compartmentalized away from nontarget tissues (e.g., lens). Furthermore, a short needle, with a length matched to the thickness of sclera (i.e., a microneedle), can be used in an outpatient procedure similar to an IVT injection.[1,8] Indeed, safety and tolerability of microneedle injection has been demonstrated in a phase I/II clinical trial (NCT01789320) in which triamcinolone acetonide was injected into SCS to treat noninfectious posterior uveitis.[1] Other indications are also actively being pursued.

When comparing pharmacokinetics of SCS against IVT injections, higher levels of injected molecules have been found in chorioretina with significantly faster clearance (on the order of hours) following SCS injection.[8,9,11,13,14] The distribution of molecules and particles injected into the SCS also have been studied to obtain a better understanding of flow within this space.[8,14–19] However, data on how fluid and molecules leave this space are less known. To date, no studies have directly investigated the clearance mechanisms from the SCS after SCS delivery. Olsen et al. examined histology of eyes after SCS injection and found that bevacizumab molecules were bound within the choroid; from this, they concluded that choroidal blood flow played a role in clearance.[11] Tyagi et al.[13] measured pharmacokinetics of molecules remaining in the eye, and concluded that choroidal blood flow was a reasonable route of clearance based on its high perfusion rate. Abarca et al.[5] measured the pharmacokinetics of molecules remaining in the eye of a postmortem pig with and without choroidal perfusion and found that clearance with perfusion was faster. These

studies only looked for the role of the choroid in clearing the SCS and concluded that it did play a role. However, the role of other routes of clearance were not considered, and no comparative quantification of the roles of various routes of clearance from SCS have been reported before.

The purpose of this work was to measure clearance kinetics and identify dominant routes of clearance from rabbit SCS after microneedle injection. We chose to study possible routes of clearance from the eye in a systematic way, referring to classical experiments to determine reasonable routes.[20–23] We hypothesized that clearance of fluid and dissolved molecules injected into SCS occurs initially through leakage sites across sclera (i.e., injection site and perivascular drainage) and via transport into choroid and scleral tissues. Later, the clearance process is completed by transport across sclera into the subconjunctival space and clearance into the systemic circulation by choriocapillaries.

Methods

All reagents and chemicals were purchased from Sigma-Aldrich Corp. (St. Louis, MO, USA) unless otherwise specified. All experiments were performed in albino New Zealand White rabbits (Charles River, Wilmington, MA, USA) and were approved by the Georgia Institute of Technology Institutional Animal Care and Use Committee. Practices complied with the ARVO Statement for the Use of Animals in Ophthalmic and Vision Research.

Microneedle Injection

Rabbits were anesthetized with isoflurane, and an eye drop of proparacaine (Bausch & Lomb, Rochester, NY, USA) was given as a topical anesthetic before injection. For all experiments, a 50-μL injection was performed into the SCS of each eye with a 33-gauge microneedle approximately 750 μm in length (kindly provided by Clearside Biomedical, Alpharetta, GA, USA) and a 1-mL syringe. All injections were made in the supranasal quadrant 3 mm posterior to the limbus and 4 mm nasal to the superior rectus muscle. Four eyes of four animals were used in each group unless otherwise specified. The 50-μL injection occurred in 3 seconds. After injection, the needle was kept in place for 1 minute to limit reflux at the injection site.

Determination of SCS Collapse Rate by Ultrasonography

High-frequency ultrasound B-scan (U/S; UBM Plus, Accutome, Malvern, PA, USA) was used to determine the rate of SCS collapse after microneedle injection of 50 μL Hank's Balanced Salt Solution (HBSS; Mediatech, Manassas, VA, USA) into SCS. Serial images were acquired every minute for 10 minutes, and then every 2 minutes for 1 hour. Off-line post processing was performed on U/S views to determine SCS thickness so the characteristic time of SCS collapse could be determined. See Supplementary Material for details.

Determination of SCS Clearance Kinetics by Fundus Imaging

To study effects of molecular radius on clearance from SCS, a 50-μL microneedle injection of the following formulations was tested: (1) 0.025% (wt/vol) fluorescein sodium; (2) 0.5% (wt/vol) 70 kDa FITC-dextran; (3) 0.5% (wt/vol) 500 kDa FITC-dextran; (4) 0.5% (wt/vol) 2 MDa FITC-dextran; (5) 1.5% (wt/vol) FITC-bevacizumab; and (6) 1% (wt/vol) 20 nm green-fluorescent particles (Excitation: 505 nm, Emission: 515 nm; FluoSpheres; Life Technologies, Carlsbad, CA, USA), all formulated in HBSS. These concentrations were chosen so the fluorescent intensity did not oversaturate the fundus camera sensor. Before injection, FITC was tagged to bevacizumab using methods described in the Supplementary Material.

The clearance rate of injected fluorescent material from SCS was estimated by taking fluorescence fundus images over time. Topical eye drops of tropicamide and phenylephrine (Akorn, Lake Forest, IL, USA) were administered before each imaging session to dilate the pupil. A RetCam II (Clarity Medical Systems, Pleasanton, CA, USA) with the 130° lens attachment and the built-in fluorescein angiography module was used to acquire images. Serial fundus collages were acquired for $\leq$28 days.

Intraocular Pressure Measurements

A custom-designed pressure measurement system was used to measure pressure in vitreous humor (VH) and in SCS after either IVT or SCS injection (see Supplementary Materials). The animal was terminally anesthetized by subcutaneous injection of a ketamine/xylazine cocktail. After SCS or IVT injection (n = four per injection site), pressure in the SCS and VH was alternatively measured every few minutes. Pressures were monitored until they had reached their original baseline values from before injection (i.e., ~15 mm Hg). After the measurements, the animal was euthanized with a lethal dose of pentobarbital injected intravenously. A second set of SCS and IVT injections was made in the animal postmortem. In postmortem measurements, pressure was measured only in the tissue space (i.e., SCS or VH) where the injection was made.

Collection of Fluorescein by Different Clearance Routes

For this terminal experiment, the rabbit (n = four eyes per group) was anesthetized with a subcutaneous injection of ketamine/xylazine before microneedle injection; additional injections were given every 30 minutes to maintain anesthesia. Subcutaneous injection of 60 mL saline was also given on the rump to counteract fluid loss. The amount of fluorescein exiting the eye was determined by collecting samples over time from [i] sclera anterior to the equator; [ii] anterior sclera with injection site plugged; [iii] sclera posterior to the equator; and [iv] posterior sclera with vortex vein transected.

Before microneedle injection, the supranasal conjunctiva was dissected off the sclera. A 50-μL microneedle injection was performed 4 mm nasal to the superior rectus muscle and 3 mm posterior to the limbus. In [i] anterior sclera and [iii] posterior sclera conditions, samples were collected for 1 hour by swabbing the space with a 1 × 1-cm paper tissue (Kimwipe; Kimberley-Clark, Irving, TX, USA). Care was taken to swab only anterior or posterior to the equator, depending on the condition. The tissue was then placed in 1 mL HBSS until analysis.

To determine the amount of fluorescein leaving [ii] the anterior sclera with injection site plugged, a similar experiment was performed. Immediately after injection, the injection site was plugged by sealing the microneedle into sclera with cyanoacrylate glue (Loctite 4013; Henkel Adhesives, Düsseldorf, Germany). Other methods were the same as above.

For eyes that had a vortex vein cut [iv], the superior vortex vein was transected before injection. Heparin (5 mL of 10,000 IU/mL; Hospira, Lake Forest, IL, USA) was given intravenously before the start of the experiment to prevent coagulation. The superior rectus muscle was lifted off the ocular surface to expose the vortex vein, which was confirmed by verifying its

Investigative Ophthalmology & Visual Science

path (i.e., originating from within sclera and traveling posteriorly along the ocular surface toward the optic nerve). A transfer pipette was used to collect blood exiting the vortex vein for 1 hour. The volume of collected blood was recorded, and HBSS was added to reach a final volume of 2 mL per sample for analysis.

Immediately after the last time point, all animals were euthanized by injection of pentobarbital through the marginal ear vein. Eyes were enucleated to determine the amount of fluorescein remaining within the tissue (including SCS), and in aqueous humor, VH, and lens. The Kimwipe paper tissue and ocular tissue samples were placed in HBSS at 4°C for 2 days to allow fluorescein to diffuse out and equilibrate with the HBSS. The amount of fluorescein in all samples was measured using a multiplate reader (Excitation: 494 nm, Emission: 521 nm; Synergy H4; BioTek, Winooski, VT, USA). In a separate experiment involving incubation of Kimwipes in a known amount of fluorescein, we found no evidence of loss in extracting fluorescein from the Kimwipe, and no leaching of fluorescent species out of the Kimwipe (data not shown).

Data and Statistical Analysis

Prism and MATLAB software were used to perform data and statistical analysis. Data were fit to exponential decays to find relevant parameters (e.g., time constant) using the formula $y(t) = Y_0 e^{(-t/\tau)}$, where t is time postinjection, $y(t)$ is SCS thickness or fluorescent-molecule fluorescence at time t, Y_0 is maximum SCS thickness or fluorescence, and τ is characteristic time constant of SCS collapse or fluorescent molecule clearance. Other data were fit to an exponential approach function, $N(t) = N_0(1 - e^{(-t/\tau)})$, where t is time postinjection, $N(t)$ is cumulative amount of fluorescein collected at time t, N_0 is maximum amount of fluorescein, and τ is characteristic time constant.

All values are reported either as mean ± SEM, or mean and 95% confidence interval (mean [95% CI]), unless otherwise specified. One-way ANOVA analysis was performed to determine statistical significance ($\alpha = 0.05$) among multiple conditions. F test was used to compare parameters generated by curve fits.

Modeling Clearance From the SCS

We developed a two-dimensional model (2D) of small-molecule transport after microneedle injection into SCS to corroborate our experimental results. This model used a modified random walk algorithm to study position and disposition of molecules by displacing the molecule at each time point in 2D based on the characteristic diffusional length a molecule would move in that period, as well as additional tissue-specific rules (see Supplementary Materials).

Results

Suprachoroidal Space Collapse Rate as a Measure of Fluid Clearance Rate From the SCS

We determined SCS collapse rate in live rabbits after microneedle injection of HBSS into the SCS (Fig. 1). Under typical conditions before injection, sclera and choroid in rabbits were apposed, because the SCS is normally collapsed (Fig. 1A, pre). On microneedle injection, fluid was introduced into the SCS, which caused the choroid to distend and lift off the sclera. This created a gap between sclera and choroid when viewed under ultrasound B-scan (Fig. 1A, 1 minute), which we tracked over time and used as a proxy for SCS collapse rate and fluid clearance rate. Because SCS expansion due to HBSS can be measured directly in this way, no tracers or contrast agents were added to the fluid.

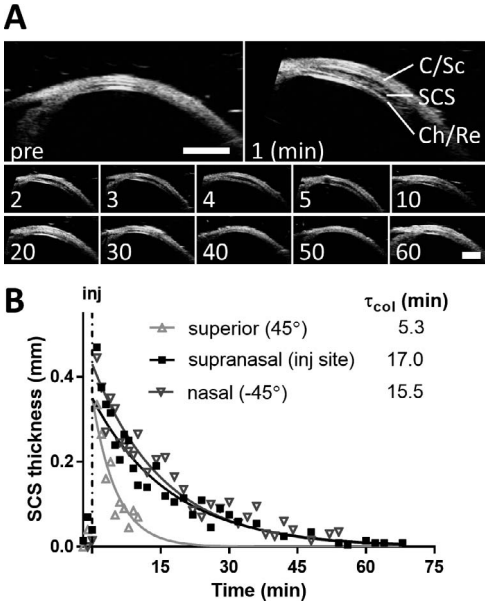

Figure 1. Suprachoroidal space thickness over time determined by ultrasound B-scan images acquired during supranasal injection of 50 µL HBSS into SCS of living rabbits. (**A**) Representative B-scans of time course. C/Sc, conjunctiva/sclera; SCS, expanded suprachoroidal space; Ch/Re, choroid/retina interface. *Scale bar*: 1 mm. (**B**) Quantification of SCS thickness (mean only, $n = 2$–6 replicates) 2 mm posterior to scleral spur at three locations. Standard error of the mean for all time points ranged from 0.00 to 0.21 mm with a mean of 0.06 mm. Reported time constants (τ_{col}) were derived from exponential-decay curve fitting.

After 50 µL injection in the supranasal position, we tracked collapse of SCS as a function of time directly over the injection site and also superiorly and nasally (Fig. 1B). Data were fit to an exponential decay ($r^2 = 0.62$–0.71). One minute after injection, SCS thickness over the injection site was 470 ± 60 µm (mean ± SEM). The collapse time constant (τ_{col}) was 19 minutes (15–27 minutes 95% CI). Suprachoroidal space expansion was indistinguishable from preinjection thickness by 40 minutes postinjection. There was no significant difference in curve fits for measurements made supranasally or nasally ($P = 0.89$, F test). Collapse rate of the superior SCS ($\tau = 5.5$ minutes [3.9–9.4 minutes]) was significantly faster than at the other two positions measured ($P < 0.05$, F test). This could be due to nearby perivascular drainage routes, but more experiments are warranted to explore this hypothesis.

Clearance Rate of Fluorescent Molecules From the SCS

We determined clearance rates of different-sized fluorescent molecules and a fluorescent nanoparticle (20-nm diameter) injected as solutions into the SCS of live rabbits. The molecules ranged in molecular weight from 332 Da (fluorescein) to 2 MDa (FITC-dextran), which corresponds to effective molecular diameters of roughly 1 nm[24] to 54 nm,[25,26] respectively. Brightfield and fluorescence fundus images were acquired for each fluorescent molecule tested over time (Fig. 2). Because the rabbits were albino, the eyes were unpigmented, which made choroidal vessels readily visible beneath the inner retinal vessels (Fig. 2, pre [brightfield]). Furthermore, there was no detectable green autofluorescence with the light level used (Fig. 2, pre).

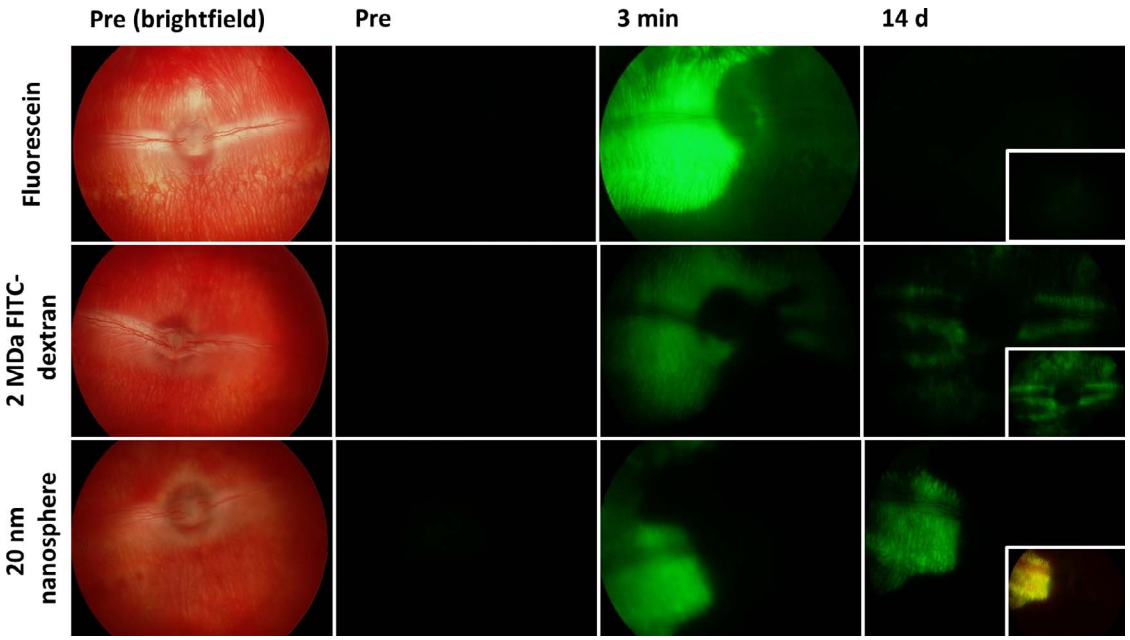

Figure 2. Representative brightfield and fluorescent fundus images of live rabbit eyes before, 3 minutes post- and 14 days postinjection of 50 μL fluorescein, 2 MDa FITC-dextran, or 20 nm polystyrene particles. Three minutes postinjection, fluorescein and 2 MDa FITC-dextran were distributed approximately equally. At all time points, nanospheres occupied less area than other formulations. The 2 MDa FITC-dextran is still visible 14 days postinjection. Nanoparticles were visible for at least 2 months (data not shown). *Inset* depicts fundus image taken under brighter light setting, enabling visualization of regions with lower level of fluorescence. All eyes oriented such that up is superior (sup.) and nasal is left (nas.). Fundus field of view is 130°.

After injection, fluorescent molecules and nanoparticles were visible in SCS (Fig. 2, 3 minutes and 14 days); localization in SCS (i.e., behind the choroid) was confirmed by shadowing of choroidal vessels over the green fluorescence. Three minutes after injection, fluorescein in HBSS and 2 MDa FITC-dextran in HBSS distributed similarly in SCS, occupying 56% ± 6% and 58% ± 7% of the visible SCS respectively ($P = 0.95$, Dunnett's test). These results were similar to the distribution seen in a previous study.[14] Both fluorescein and 2 MDa FITC-dextran covered larger areas of SCS than the nanoparticles (28% ± 6%; $P < 0.05$, Dunnett's test).

We further determined rate of clearance by determining total clearance time and clearance time constant ($\tau_{clearance}$) calculated using a curve fit derived from the normalized concentration of total fluorescent signal over time. We defined total clearance time as the first time point after injection in which fluorescence was not detected in fundus images with the middle light intensity. Representative time courses for fluorescein (Figs. 2, upper row, 3A) and 2 MDa FITC-dextran (Figs. 2, middle row, 3B) show rates of clearance and calculated total clearance time. In the representative images in Figures 2A and 2B, fluorescein is not visible by 1 day, whereas 2 MDa FITC-dextran was not totally cleared until 21 days.

Fluorescence was tracked via fundus examinations with a series of lighting conditions, and used to estimate relative concentration of fluorescent molecules over time in SCS. For each fluorescent molecule, data were fit to an exponential decay ($r^2 > 0.84$; Fig. 3C). Time constants from curve fits are shown in Figure 3D (closed squares), along with total clearance time (Fig. 3D, open circles) for all fluorescent species tested.

Clearance time constant was linearly dependent on molecular diameter (Fig. 3D, $r^2 = 0.87$), varying from 4.3 ± 0.4 hours for fluorescein and 26.0 ± 9.8 hours for 2 MDa FITC-dextran. Total clearance time also could be fit to a line (Fig. 3D, $r^2 = 0.43$), but appeared to show nonlinearity at high molecular size. Although clearance time constant had a value similar to total clearance time for the smaller molecules, total clearance time was greater for the larger molecules, suggesting a biphasic clearance rate for which a fraction of the larger molecules persisted in SCS for a longer time. Nanoparticles were not cleared from SCS for the duration of the study (>2 months). Despite differences in molecular weight and chemical structure between FITC-dextran and FITC-bevacizumab, clearance times were similar due to comparable hydrodynamic diameter of 70 kDa FITC-dextran[24] (~12 nm) and FITC-bevacizumab[24,27] (~11 nm), consistent with a dominant role of molecular diameter in determining SCS clearance.

Intravitreal and SCS Pressure Measurements

Vitreous humor pressure trace after IVT injection was consistent with prior literature, showing a roughly exponential decay in pressure that returned to within 10% of baseline value within 15 minutes.[18,28] Furthermore, VH pressure after SCS injection followed a similar time course, returning to within 10% of baseline value by 15 minutes. Vitreous humor and SCS pressure traces were within ±1 mm Hg of each other throughout the length of the experiment. Thus, we conclude that the time course of pressure decay in the eye is the same after IVT or SCS injection.

Each data set was fit to an exponential decay, from which a pressure-decay time constant ($\tau_{pressure}$) was calculated (Fig. 4). There was no significant difference among any of the four time constants derived from VH and SCS pressure curve fits after IVT or SCS injection in vivo ($P = 0.98$, 2-way ANOVA).

Injections made postmortem in companion eyes resulted in significantly faster depressurization (~1 minute) than injections in vivo ($P < 0.05$, 2-way ANOVA). Because eyes were not enucleated and tissue degradation had likely not yet happened, we believe the main difference between in vivo eyes and postmortem eyes is lack of living processes, such as choroidal

Investigative Ophthalmology & Visual Science

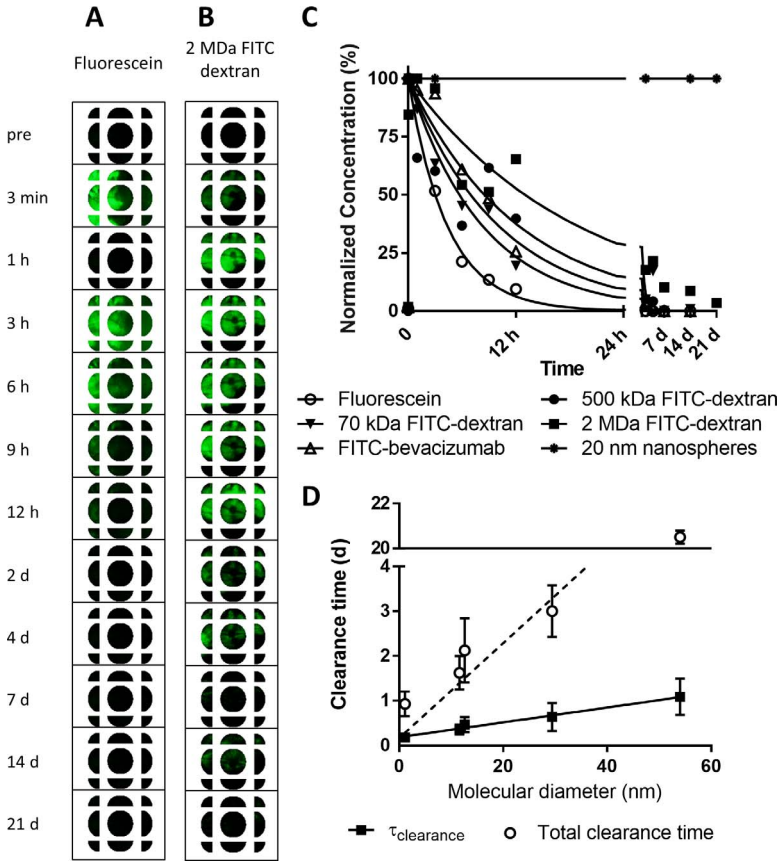

Figure 3. Analysis of rates of clearance from SCS after 50 μL SCS injection with molecules ranging from 1 to 60 nm in diameter and a 20-nm polystyrene particle. (**A**) Representative fundus collages after injection with fluorescein in HBSS. (**B**) Representative fundus collages after injection with 2 MDa FITC-dextran in HBSS. (**C**) Quantification of fluorescein/FITC- concentration with curve fit to an exponential decay. (**D**) Clearance time constant ($\tau_{clearance}$, from curve fit in [**C**]) and total clearance time plotted against hydrodynamic molecular diameter. Nominal molecular diameters are 1.1 nm for fluorescein,[24] 11.6 nm for 70 kDa FITC-dextran, 12.6 nm for FITC-bevacizumab,[27] 29.4 nm for 500 kDa FITC-dextran,[40] and 54 nm for 2 MDa FITC-dextran.[26] All values are mean ± SEM ($n = 3$–7 eyes).

perfusion. Possible explanations include increased perivascular drainage (because the vortex vein is collapsed with no blood flow), or that blood volume was expelled from the eye on SCS injection (as there was minimal resistance to venous flow and no refilling of ocular vascular beds).

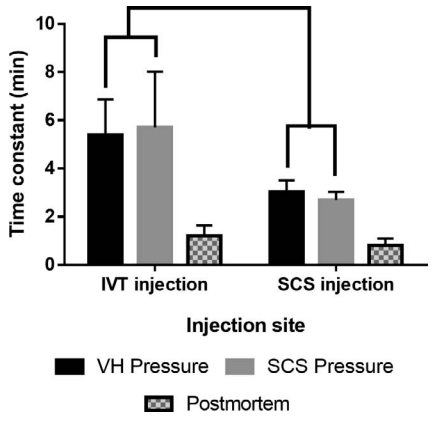

Figure 4. Pressure measurement in vivo and postmortem after SCS injection of 50 μL HBSS. Pressure-decay time constants derived from fitting data to exponential decays. There was no significant difference in time constants from SCS or VH pressure traces after SCS or IVT injections in vivo. In vivo time constants were different from postmortem time constants. All values are mean ± SEM ($n = 4$ replicates).

Route of Clearance After SCS Injection

To assess contributions of different routes of clearance, we collected fluorescein from multiple collection sites after SCS injection in vivo (Fig. 5). The fluorescein collected from these collection sites was determined over time (Fig. 5B). The amount of fluorescein leaving through the injection site (Fig. 5B, upper right) was found by subtracting site [i] from site [ii] (i.e., difference in fluorescein collected from sclera anterior to the equator without and with injection site plugged). And the amount of fluorescein leaving through blood (Fig. 5B, lower right) was found by subtracting site [iv] from site [iii] (i.e., difference in fluorescein collected from sclera posterior to the equator with and without the vortex vein transected). Although the physiological data are inherently noisy, they should nevertheless enable an order of magnitude characterization of the underlying processes (which can be compared with a theoretical model of transport below). The amount of fluorescein collected over time also was found (Fig. 5C).

Cumulative amount of fluorescein collected at 1 hour, as well as residual amounts in ocular tissues, were calculated and expressed as a function of total fluorescein injected into SCS (Fig. 5D). One hour postinjection, 46% ± 18% was still within tissue (e.g., in sclera, choroid, SCS); 15.0% ± 0.3% had passed transsclerally to the subconjunctival space (anterior and posterior combined); and 6.3% ± 4.0% was found in blood. We calculated that 1.3% ± 4.0% exited via the injection site and 2.5% ± 0.3% exited via perivascular drainage around the

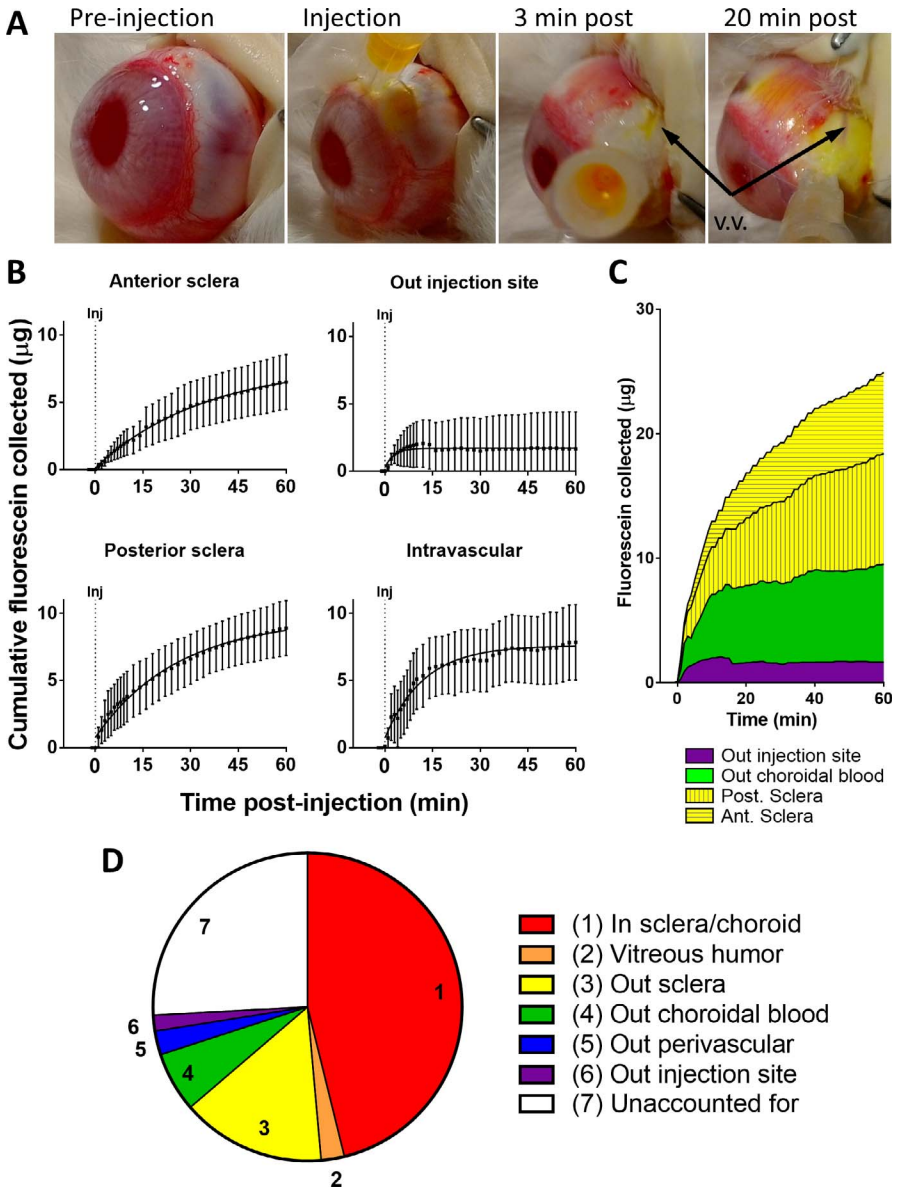

Figure 5. Fluorescein collected from four routes out of SCS after 50 μL SCS injection of fluorescein in HBSS. (**A**) Representative series of images of eye with injection site plugged. (**B**) Cumulative fluorescein collected by swabbing anterior sclera after plugging injection site (**B**, upper left), collected by swabbing posterior sclera (**B**, lower left), calculated by comparing amount collected from anterior sclera with and without plugging injection site (**B**, upper right), and calculated by comparing amount collected from posterior subconjunctiva with and without transecting vortex vein (**B**, lower right). All values are mean ± SEM ($n = 4$ replicates). (**C**) Total fluorescein collected over time by adding up data in (**B**). (**D**) Quantification of total fluorescein distribution in and out of the eye after SCS injection based on data in (**B**) and analysis of residual fluorescein content in the eye after enucleation.

vortex vein. We were unable to account for 28% of the fluorescein, which might be due to collection error.

Modeling Clearance From the SCS

At time t = 0, 1000 molecules were randomly "injected" into SCS (Fig. 6A[ii]). At each subsequent time point (time step $\Delta t =$ 1 minute), molecules were moved following the rules described above depending on each molecule's location at the previous time point (Fig. 6A). Location and fate of each molecule was recorded (i.e., in the eye, outside sclera, or cleared via choroid).

After 5 minutes (Fig. 6A[iii]), more than 95% of molecules had left the SCS. A fraction of the molecules was rapidly convected across sclera via leakage pathways at the site of injection and via perivascular routes (treated in the simulation as a single shunt pathway through the center of sclera, as depicted in Fig. 6A[i]). The remaining molecules were transported into choroid or sclera as SCS collapsed (in the simulation, SCS did not collapse). Transport into the choroid was exclusively by diffusion, because no pressure gradient from SCS across choroid was expected. Transport into sclera (i.e., not via leakage pathways) was through a combination of diffusion and convection driven by the decaying pressure gradient across sclera.

Within 15 minutes after injection (Fig. 6A[iv]), molecules penetrated deeper into choroid and sclera, and began to be cleared from these tissues. At 1 hour (Fig. 6A[v]), most molecules within the choroid had been cleared into the bloodstream, whereas molecules in the sclera continued to be

Investigative Ophthalmology & Visual Science

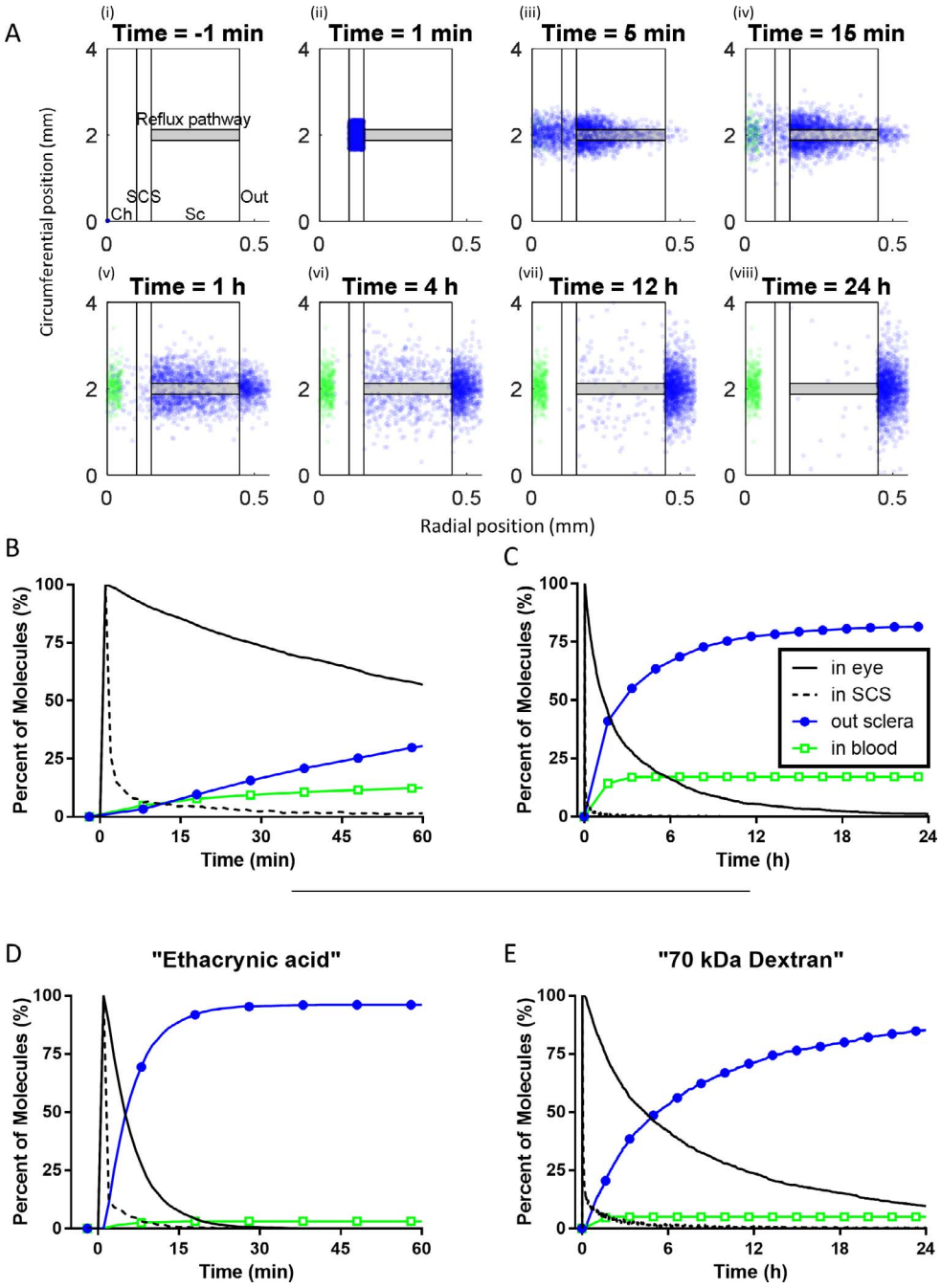

Figure 6. Results from theoretical model of molecule transport in SCS. Transport after SCS injection with (**A**–**C**) "fluorescein"; (**D**) molecule with no binding, "ethacrynic acid"; and (**E**) high-molecular-weight molecule, "70 kDa dextran." (**A**) Cross-sectional view of eye showing position of molecules (*blue dots*) and molecules that were cleared in blood (*green dots*) at different times postinjection. Ch, choroid; Sc, sclera. Percentage of particles found in the eye, in SCS, on the exterior surface of sclera, and in the blood via the choroid (**B**) within 1 hour after injection and (**C**) within 24 hours after injection. Summarized fate of (**D**) small molecule that does not bind sclera and (**E**) large molecule, 70 kDa dextran.

cleared. The rate of clearance from choroid was determined by the rate of diffusion of molecules to capillaries and the odds of being taken up by a capillary. At 4 and 12 hours (Figs. 6A[vi], [vii]), transport across the sclera continued. Rate of clearance from the sclera was determined by the rate of transport to the outer scleral surface by diffusion, as well as convection driven by the normal IOP of the eye (i.e., 15 mm Hg in the rabbit). Our model, as well as previous literature,[29] predicted that both of these driving forces may play a role in transscleral transport.

By 24 hours (Fig. 6A[viii]), the clearance process was largely complete. Snapshots shown in Figure 6A were supplemented with continuous time course results over the course of 1 hour (Fig. 6B) and 1 day (Fig. 6C). Note that this modeling result was for the low-molecular weight compound fluorescein that bound to tissue (Figs. 6A–C). We predict that molecules that do not bind (e.g., ethacrynic acid[30] [Fig. 6D]), or have higher molecular weight (e.g., 70 kDa dextran [Fig. 6E]), would be cleared similarly, but with different kinetics, especially for diffusion-based processes.

The model suggests that sclera accounted for more clearance than choroid. This could be explained as follows. After injection into SCS, a molecule experienced isotropic

Investigative Ophthalmology & Visual Science

diffusion (recall that there was no pressure differential in the eye interior to sclera) and was thus able to diffuse either circumferentially within SCS or radially (toward choroid or toward sclera) at similar rates. Circumferential diffusion did not affect clearance much, but radial transport played a major role in a molecule's eventual clearance route. If the molecule diffused into sclera, there was sufficient diffusive transport and convective flow due to physiological IOP across sclera to ensure clearance of the molecule across the thickness of sclera. Alternatively, if the molecule diffused into choroid, the molecule had a probability of clearing via choriocapillaries. However, if the molecule within choroid did not clear immediately, it could diffuse toward sclera and consequently become driven transsclerally. Approximately one-third of molecules that diffused into choroid initially were eventually cleared through sclera.

Exponential curve fits were generated from model results in Figure 6C. The percentage of molecules found in the eye was fit to a first-order exponential decay, which yielded a time constant of 3.38 hours (95% CI 3.34–3.41) ($r^2 = 0.98$). Cumulative percentage of molecules that had entered the blood via choroid was fit to a first-order exponential approach function with a time constant of 0.93 hour (0.92–0.94) ($r^2 = 0.99$). Cumulative percentage of molecules that had exited the eye via transscleral transport routes was fit to a first-order exponential approach with a time constant of 3.84 hours (3.80–3.87) ($r^2 = 0.99$).

Sensitivity Analysis and Effect of Parameters

We also modeled behavior of a small molecule that did not bind to sclera[30] and a large molecule,[24] as summarized in Figures 6D and 6E, respectively. To model a small molecule that did not bind sclera, we used experimentally derived values for ethacrynic acid; in particular, we increased diffusivity to 5×10^{-6} cm^2/s and decreased B_{max} to 5 μM (other parameters were kept the same as the fluorescein condition).[30] The model predicted that half-life of "ethacrynic acid" in the eye to be 4.8 minutes with complete clearance by 25 minutes (Fig. 6D). These values were similar to SCS collapse time (which could be viewed as a proxy for clearance of water from SCS). Comparison of these characteristic times with those for fluorescein showed the dramatic effect that binding can have on clearance rates.

Clearance of a large macromolecule was modeled using values experimentally determined for 70 kDa FITC-dextran. In particular, we decreased diffusivity to 5×10^{-8} cm^2/s (by assuming experimentally derived scleral permeability of 1.5×10^{-6} cm/s[24] was at steady state across the thickness of sclera), decreased choroidal clearance rate to 0.005 min^{-1} (because larger molecules should have more difficulty passing through fenestrae of the choriocapillaris[31]), and decreased binding affinity B_{max} to 1000 μM (Ref. 24) while keeping other parameters the same as the fluorescein condition. The model predicted the half-life of this macromolecule to be 5.2 hours and total clearance time to be 3.8 days. Both values were within a factor of two of values we found experimentally. For all three model molecules tested, dominant route of clearance was via transscleral transport with a lesser contribution from intravascular clearance in choroid.

Sensitivity analysis of model parameters and critique of limitations of the model can be found in the Supplementary Material.

Discussion

In this study, we investigated clearance kinetics of molecules injected into the SCS of live rabbits using a microneedle.

Table. Characteristic Times of Transport Phenomena in the Eye

Characteristic Time, Order of Magnitude	Transport Phenomena in Eye
1 min	• SCS loaded with fluid and molecules during injection
10 min	• Fluid and molecules cleared from SCS by convection through leakage pathways • Remaining molecules transported into choroid and sclera • SCS collapses • IOP drops to baseline
1 h	• Molecules cleared by choroidal blood flow
1–10 h	• Molecules cleared from sclera by diffusion and convection

Previous studies demonstrated decay of IOP after SCS injection on a time scale of minutes,[18] which is expected to correlate with the time scale of fluid clearance from SCS, and reported clearance of various molecules from SCS on a time scale of hours,[7–9,11,13,17] both of which we corroborated in this study. Previous studies also have found that clearance times after suprachoroidal delivery were significantly faster than after IVT injections.[32] We also found that complete collapse of SCS occurred by 40 minutes, which is consistent with previous studies.[17,33] During the first hour postinjection, approximately half of injected fluorescein was cleared from the ocular globe, with approximately half still remaining. The remaining fluorescein was not visible by 12 hours postinjection.

Dominant Route of Clearance From the SCS

Because the time constants of molecule clearance from the eye and the time constant of transscleral clearance were of the same order of magnitude of hours (with intravascular clearance being significantly faster), the model suggested that transscleral diffusion was the dominant route of clearance. The model generated a clearance time constant similar to the time constant of 4.3 hours that we found based on fundus imaging (Fig. 2).

Guided by experimental data in the context of model predictions, characteristic times of key transport phenomena following SCS injection are summarized in the Table.

Effect of Molecular Size on Residence Time

We found experimentally and computationally that increasing molecular radius had a major effect on clearance time. Fluorescein (~1 nm in diameter[24]) was cleared by 24 hours, while 2 MDa FITC-dextran (~50 nm in diameter[25]) was not fully cleared until 21 days. The prolonged residence time did not increase linearly with molecular mass, but was dramatically longer above a threshold of approximately 10^6 Da. The difficulty for very large macromolecules to pass through fenestrae of the choriocapillaris and through extracellular matrix of sclera is the likely explanation for this behavior.

As shown in this study, the bulk of clearance occurred via diffusion across sclera, as well as through choroid into choriocapillaries. The physiological upper limit of pore size of the choriocapillaris is estimated to be approximately 6 nm.[31] Thus, the hydrodynamic radius of 2 MDa FITC-dextran is much larger than choriocapillaris pore size. Because macromolecules are not rigid, even 2 MDa FITC-dextran can eventually adopt a conformation that allows passage through fenestra of a choriocapillary. On the other hand, small polystyrene microspheres (20 nm in diameter), which are rigid and are not able to adopt different conformations, were still visible on fundus

Investigative Ophthalmology & Visual Science

examination 2 months after injection.[8,16] Diffusion across sclera is the other main mechanism for clearance. Experimental studies and theoretical analysis have shown that scleral permeability decreases as a steep function of molecular mass.[34,35]

Implications for Drug Delivery

The findings in this study may be instructive for controlling drug delivery via the SCS. The observation that pressure-driven flow occurs through leakage sites indicates the importance of minimizing leaking from the site of injection (e.g., by keeping the microneedle in place after injection). It also suggests that there are diminishing returns on increasing injection volume; larger volumes lead to larger IOP, which lead to more loss of fluid through pressure-driven flow through leakage pathways.

Most molecules injected in SCS are cleared into systemic circulation via the choriocapillaris or transsclerally into the subconjunctival space. Drugs cleared via choroid can interact with possible drug targets in that tissue, and possibly diffuse across RPE into retina, where additional drug targets are also located. Drugs cleared across sclera (or via leakage pathways) do not enter choroid or retina, and therefore do not reach targets in those tissues.

Residence time in SCS depends on what is injected. It has previously been reported that molecules are cleared from SCS within 1 day and that particles are not cleared at all.[3,8,9,11,13,17] This study corroborated those findings, which suggests that extending residence time of drugs in SCS requires their incorporation into particulate controlled release systems.[12] However, this study also suggests a new approach, which involves use of drug molecules of very high molecular mass, possibly by affinity-binding or conjugation to a large polymer, use of a prodrug, or other strategies.[36–39]

To our knowledge, this is the first study to provide experimental and computational evidence of relative contributions of different routes of clearance from SCS. In particular, we considered pressure-driven flow through leakage routes (e.g., perivascular leakage routes and reflux out the injection site) and transscleral transport; and diffusion-mediated transport across sclera and into choroid for intravascular clearance. We also identified timescales and relative contributions of each of these routes of clearance for the first time.

Limitations

There were several limitations to this study. There are anatomical and physiological differences between rabbit and human eyes. Human clinical trials will be needed if these findings are to be applied to human medicine; however, sensitivity analysis indicates that changes in hydraulic conductivity and scleral thickness did not have major effects on the results of the model (see Supplemental Material). Another possible concern is that we have an incomplete mass balance from fluorescein collection experiments (i.e., 28% unaccounted for in Fig. 5). Although we assume that incomplete capture occurred equally in all collection routes, it is possible this collection was biased (i.e., unequal loss of fluorescein from the different routes, especially the intravascular route that was most difficult to collect). Because this study was performed with fluorescent tracer molecules and not a real drug, pharmacokinetic studies with drugs of interest are needed.

Conclusions

In summary, we used live New Zealand White rabbits to study molecular clearance from SCS after microneedle injection. Previous studies demonstrated the importance of choroidal perfusion on clearance with no mention on other routes[5,11,13]; thus, no conclusion could be drawn about SCS clearance mechanisms. In this study, we identified that clearance occurs in three regimes. (1) There was immediate loss of fluorescein from pressure-driven leakage at the injection site and via perivascular routes associated with vortex veins on a time scale of minutes, which accounted for a few percent of clearance from SCS under the conditions of this study. The remaining molecules were transported out of SCS and into sclera or choroid. (2) Concentration-driven diffusion into choroid and subsequent clearance by choriocapillaries took place on a time scale of an hour. (3) Diffusion and physiological IOP-mediated convection across sclera cleared remaining fluorescein from the eye over the course of hours. These experimental data were supported by a theoretical model of small-molecule transport in the eye. Increasing molecular radius of injected molecules significantly slowed rate of clearance. These experiments can guide development of strategies to better control drug delivery via the SCS.

Acknowledgments

The authors thank Henry Edelhauser, Timothy Olsen, and Pradnya Samant for helpful discussions; Jae Hwan Jung and Brandon Gerberich for assistance with experiments; Machelle Pardue for use of the RetCam; and Donna Bondy for administrative support. This work was carried out at the Institute for Bioengineering and Bioscience and Center for Drug Design, Development and Delivery at Georgia Tech.

Supported by National Eye Institute grants EY017045 (BC, MRP), EY022097 (BC, MRP), EY007092 (BC), and EY025154 (BC).

Disclosure: **B. Chiang**, P; **K. Wang**, None; **C.R. Ethier**, None; **M.R. Prausnitz**, Clearside Biomedical (I, S), P

References

1. Goldstein DA, Do D, Noronha G, Kissner J, Srivastava SK, Nguyen Q. Suprachoroidal corticosteroid administration: a novel route for treatment of noninfectious uveitis. *Trans Vis Sci Tech*. 2015;5(6):14.
2. Chen M, Li X, Liu J, Han Y, Cheng L. Safety and pharmacodynamics of suprachoroidal injection of triamcinolone acetonide as a controlled ocular drug release model. *J Control Release*. 2015;203:109–117.
3. Patel SR, Lin AS, Edelhauser HF, Prausnitz MR. Suprachoroidal drug delivery to the back of the eye using hollow microneedles. *Pharm Res*. 2011;28:166–176.
4. Olsen TW, Feng X, Wabner K, et al. Cannulation of the suprachoroidal space: a novel drug delivery methodology to the posterior segment. *Am J Ophthalmol*. 2006;142:777–787.
5. Abarca EM, Salmon JH, Gilger BC. Effect of choroidal perfusion on ocular tissue distribution after intravitreal or suprachoroidal injection in an arterially perfused ex vivo pig eye model. *J Ocul Pharmacol Ther*. 2013;29:715–722.
6. Kadam RS, Williams J, Tyagi P, Edelhauser HF, Kompella UB. Suprachoroidal delivery in a rabbit ex vivo eye model: influence of drug properties, regional differences in delivery, and comparison with intravitreal and intracameral routes. *Mol Vis*. 2013;19:1198–1210.
7. Tyagi P, Barros M, Stansbury JW, Kompella UB. Light-activated, in situ forming gel for sustained suprachoroidal delivery of bevacizumab. *Mol Pharm*. 2013;10:2858–2867.
8. Patel SR, Berezovsky DE, McCarey BE, Zarnitsyn V, Edelhauser HF, Prausnitz MR. Targeted administration into the suprachoroidal space using a microneedle for drug delivery to the

posterior segment of the eye. *Invest Ophthalmol Vis Sci*. 2012;53:4433–4441.

9. Wang M, Liu W, Lu Q, et al. Pharmacokinetic comparison of ketorolac after intracameral, intravitreal, and suprachoroidal administration in rabbits. *Retina*. 2012;32:2158–2164.
10. Kim YC, Edelhauser HF, Prausnitz MR. Targeted delivery of antiglaucoma drugs to the supraciliary space using microneedles. *Invest Ophthalmol Vis Sci*. 2014;55:7387–7397.
11. Olsen TW, Feng X, Wabner K, Csaky K, Pambuccian S, Cameron JD. Pharmacokinetics of pars plana intravitreal injections versus microcannula suprachoroidal injections of bevacizumab in a porcine model. *Invest Ophthalmol Vis Sci*. 2011;52:4749–4756.
12. Chiang B, Kim YC, Doty AC, Grossniklaus HE, Schwendeman SP, Prausnitz MR. Sustained reduction of intraocular pressure by supraciliary delivery of brimonidine-loaded poly(lactic acid) microspheres for the treatment of glaucoma. *J Control Release*. 2016;228:48–57.
13. Tyagi P, Kadam RS, Kompella UB. Comparison of suprachoroidal drug delivery with subconjunctival and intravitreal routes using noninvasive fluorophotometry. *PLoS One*. 2012;7:e48188.
14. Chiang B, Venugopal N, Edelhauser HF, Prausnitz MR. Distribution of particles, small molecules and polymeric formulation excipients in the suprachoroidal space after microneedle injection. *Exp Eye Res*. 2016;153:101–109.
15. Chiang B, Kim YC, Edelhauser HF, Prausnitz MR. Circumferential flow of particles in the suprachoroidal space is impeded by the posterior ciliary arteries. *Exp Eye Res*. 2016;145:424–431.
16. Kim YC, Oh KH, Edelhauser HF, Prausnitz MR. Formulation to target delivery to the ciliary body and choroid via the suprachoroidal space of the eye using microneedles. *Eur J Pharm Biopharm*. 2015;95:398–406.
17. Gu B, Liu J, Li X, Ma Q, Shen M, Cheng L. Real-time monitoring of suprachoroidal space (SCS) following SCS injection using ultra-high resolution optical coherence tomography in guinea pig eyes. *Invest Ophthalmol Vis Sci*. 2015;56:3623–3634.
18. Kim YC, Edelhauser HF, Prausnitz MR. Particle-stabilized emulsion droplets for gravity-mediated targeting in the posterior segment of the eye. *Adv Healthc Mater*. 2014;3:1272–1282.
19. Seiler GS, Salmon JH, Mantuo R, Feingold S, Dayton PA, Gilger BC. Effect and distribution of contrast medium after injection into the anterior suprachoroidal space in ex vivo eyes. *Invest Ophthalmol Vis Sci*. 2011;52:5730–5736.
20. Moseley H, Foulds WS, Allan D, Kyle PM. Routes of clearance of radioactive water from the rabbit vitreous. *Br J Ophthalmol*. 1984;68:145–151.
21. Moseley H, Foulds WS. The movement of xenon-133 from the vitreous to the choroid. *Exp Eye Res*. 1982;34:169–179.
22. Inomata H, Bill A. Exit sites of uveoscleral flow of aqueous humor in cynomolgus monkey eyes. *Exp Eye Res*. 1977;25:113–118.
23. Bill A. Quantitative determination of uveal blood flow in rabbits. *Acta Physiol Scand*. 1962;55:101–110.
24. Ambati J, Canakis CS, Miller JW, et al. Diffusion of high molecular weight compounds through sclera. *Invest Ophthalmol Vis Sci*. 2000;41:1181–1185.
25. Kano MR, Bae Y, Iwata C, et al. Improvement of cancer-targeting therapy, using nanocarriers for intractable solid tumors by inhibition of TGF-beta signaling. *Proc Natl Acad Sci U S A*. 2007;104:3460–3465.
26. Dreher MR, Liu W, Michelich CR, Dewhirst MW, Yuan F, Chilkoti A. Tumor vascular permeability, accumulation, and penetration of macromolecular drug carriers. *J Natl Cancer Inst*. 2006;98:335–344.
27. Wen H, Hao J, Li SK. Characterization of human sclera barrier properties for transscleral delivery of bevacizumab and ranibizumab. *J Pharm Sci*. 2013;102:892–903.
28. Benz MS, Albini TA, Holz ER, et al. Short-term course of intraocular pressure after intravitreal injection of triamcinolone acetonide. *Ophthalmology*. 2006;113:1174–1178.
29. Rudnick DE, Noonan JS, Geroski DH, Prausnitz MR, Edelhauser HF. The effect of intraocular pressure on human and rabbit scleral permeability. *Invest Ophthalmol Vis Sci*. 1999;40:3054–3058.
30. Lin CW, Wang Y, Challa P, Epstein DL, Yuan F. Transscleral diffusion of ethacrynic acid and sodium fluorescein. *Mol Vis*. 2007;13:243–251.
31. Sarin H. Physiologic upper limits of pore size of different blood capillary types and another perspective on the dual pore theory of microvascular permeability. *J Angiogenes Res*. 2010;2:14.
32. Bakri SJ, Snyder MR, Reid JM, Pulido JS, Ezzat MK, Singh RJ. Pharmacokinetics of intravitreal ranibizumab (Lucentis). *Ophthalmology*. 2007;114:2179–2182.
33. Chiang B, Venugopal N, Grossniklaus HE, Jung JH, Edelhauser HF, Prausnitz MR. Thickness and closure kinetics of the suprachoroidal space following microneedle injection of liquid formulations. *Invest Ophthalmol Vis Sci*. 2017;58:555–564.
34. Prausnitz MR, Noonan JS. Permeability of cornea, sclera, and conjunctiva: a literature analysis for drug delivery to the eye. *J Pharm Sci*. 1998;87:1479–1488.
35. Edwards A, Prausnitz MR. Predicted permeability of the cornea to topical drugs. *Pharm Res*. 2001;18:1497–1508.
36. Conway A, Vazin T, Spelke DP, et al. Multivalent ligands control stem cell behaviour in vitro and in vivo. *Nat Nanotechnol*. 2013;8:831–838.
37. Pollock JF, Ashton RS, Rode NA, Schaffer DV, Healy KE. Molecular characterization of multivalent bioconjugates by size-exclusion chromatography with multiangle laser light scattering. *Bioconjug Chem*. 2012;23:1794–1801.
38. Stebbins ND, Faig JJ, Yu W, Guliyev R, Uhrich KE. Polyactives: controlled and sustained bioactive release via hydrolytic degradation. *Biomater Sci*. 2015;3:1171–1187.
39. Kontermann RE. Half-life extended biotherapeutics. *Expert Opin Biol Ther*. 2016;16:903–915.
40. Hussain AA, Starita C, Hodgetts A, Marshall J. Macromolecular diffusion characteristics of ageing human Bruch's membrane: implications for age-related macular degeneration (AMD). *Exp Eye Res*. 2010;90:703–710.

Investigative Ophthalmology & Visual Science